Appropriate extended functions for X-FEM simulation of plastic fracture mechanics

Thomas Elguedj, Anthony Gravouil, Alain Combescure

Appropriate extended functions for X-FEM simulation of plastic fracture mechanics

T. Elguedj, A. Gravouil, A. Combescure *

Laboratoire de Mécanique des Contacts et des Solides, UMR 5514, INSA Lyon, Villeurbanne, France

The extended finite element method (X-FEM) was used with success in the past few years for linear elastic fracture mechanics (LEFM). In the case of elastic–plastic fracture mechanics (EPFM), this method cannot be used without adequate asymptotic solutions to enrich the shape function basis. In this paper, we propose to use the well-known Hutchinson–Rice–Rosengren (HRR) fields to represent the singularities in EPFM. The analysis we are presenting is done in the context of confined plasticity, and shall be used to predict fatigue crack growth without remeshing. A Fourier analysis of the HRR fields is done in order to extract a proper elastic–plastic enrichment basis. Several strategies of enrichment, based on the Fourier analysis results, are compared and a six-enrichment-functions basis is proposed. This new tip enrichment basis is coupled with a Newton like iteration scheme and a radial return method for plastic flow. Numerical comparisons with and without unloading of fracture parameters are made with classical finite element results and show good agreements.

Keywords: Elastic–plastic; Fracture mechanics; Extended finite element method; HRR fields

1. Introduction

This paper presents an extended finite element method (X-FEM) for fatigue fracture analysis of cracks in homogeneous, isotropic, elastic–plastic two-dimensional solids subject to mixed mode in the case of confined plasticity. The hypothesis of confined plasticity (i.e., the plasticity is confined to the region near the crack tip) is important in this study as one is to use it to predict fatigue crack growth.

* Corresponding author. Tel.: +33 4 72436426; fax: +33 4 78890980.
E-mail address: alain.combescure@insa-lyon.fr (A. Combescure).

In linear elastic fracture mechanics (LEFM), since the asymptotic solutions are known, the application of the partition of unity concept [1] in X-FEM was successful [2–4]. In recent work (see Refs. [5,6]) some authors have also proposed to replace the "classic" linear elastic tip enrichment basis with more efficient ones in their cases. Some authors have also proposed to use extended finite element/partition of unity methods to treat non-linear problems, see for example Refs. [7,8]. One proposes in this paper to extend the X-FEM to treat material non-linearities at the vicinity of cracks.

In the case of elastic–plastic fracture mechanics (EPFM), the asymptotic fields are not analytically known. The Hutchinson–Rice–Rosengren (HRR) [9,10] solutions describe the nature of the dominant singularity in the case of a power-law hardening material. Although higher order terms may have important effects [11,12] they should be insignificant in the case of confined plasticity. These fields are used to build a plastic enrichment basis that will be implemented in X-FEM, comparable to the one used for LEFM described in [13].

As unloading will be inevitable in fatigue simulation, the usual Ramberg–Osgood non-linear material representation is not sufficient to model the corresponding elastic–plastic material in the numerical computation. Therefore, the HRR fields are only used to construct the enrichment basis that will capture the plastic singularity. A Newton like iteration scheme is used to compute equilibrium in conjunction with a radial return mapping scheme to compute plastic irreversible strains.

A Fourier analysis of the HRR fields is done in order to construct the enrichment basis. One shows that a truncated expansion of these fields on the Fourier harmonics can adequately represent the complete HRR fields. An eight-functions-enrichment basis comes out of this analysis. After some numerical experiments, a basis composed of six functions only appears to be the best for X-FEM elastic–plastic mixed mode fracture analysis. It is similar to the one used in [14] within the context of the element free Galerkin method. Numerical comparisons with and without unloading with standard finite element results are presented to validate the method.

2. Study of the elastic–plastic asymptotic fields

2.1. Elastic–plastic singularities

Let us consider a power-law hardening material associated with uniaxial stress–strain (σ–ε) relationship

$$\frac{\varepsilon}{\varepsilon_0} = \frac{\sigma}{\sigma_0} + \alpha\left(\frac{\sigma}{\sigma_0}\right)^n \tag{1}$$

where σ_0 is the reference stress, $\varepsilon_0 = \sigma_0/E$ the reference strain, E the Young modulus, α a material constant and n the hardening exponent. When n equals 1 (respectively ∞) Eq. (1) represents linear-elastic (respectively rigid-perfectly plastic) material. For multiaxial stress state, the Ramberg-Osgood law can be generalized with respect to the strain rate partition

$$\dot{\varepsilon}_{ij} = \dot{\varepsilon}^{\mathrm{e}}_{ij} + \dot{\varepsilon}^{\mathrm{p}}_{ij} \tag{2}$$

where

$$\dot{\varepsilon}^{\mathrm{e}}_{ij} = \frac{1+\nu}{E}\dot{s}_{ij} + \frac{1-2\nu}{3E}\dot{\sigma}_{pp}\delta_{ij} \tag{3}$$

and

$$\dot{\varepsilon}^{\mathrm{p}}_{ij} = \frac{3}{2E}\alpha\left(\frac{\sigma_e}{\sigma_0}\right)^{n-1}\dot{s}_{ij} \tag{4}$$

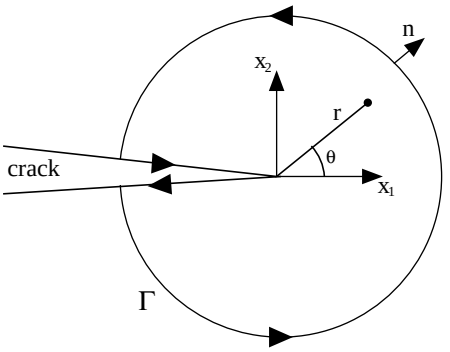

Fig. 1. Coordinates and geometry of the crack tip.

are the elastic and plastic components of strain rate, v the Poisson ratio, $\dot{s}_{ij} = \dot{\sigma}_{ij} - \dot{\sigma}_{pp}\delta ij/3$ is the deviatoric stress rate, $\sigma_e = \sqrt{3s_{ij}s_{ij}/2}$ is the Von Mises stress, and δ_{ij} the Kronecker symbol. In the fracture process zone at the vicinity of the crack tip, elastic strain rates are negligible when compared with plastic strain rates, i.e., $\dot{\varepsilon}_{ij} \simeq \dot{\varepsilon}^{\mathrm{p}}_{ij}$ and the asymptotic crack tip fields are given by Eqs. (5)–(7):

$$\sigma_{ij} = \sigma_0 \left(\frac{J}{\alpha\sigma_0\varepsilon_0 I_n r} \right)^{1/(n+1)} \tilde{\sigma}_{ij}(\theta, n) \tag{5}$$

$$\varepsilon_{ij} = \alpha\varepsilon_0 \left(\frac{J}{\alpha\sigma_0\varepsilon_0 I_n r} \right)^{n/(n+1)} \tilde{\varepsilon}_{ij}(\theta, n) \tag{6}$$

$$u_i = \alpha\varepsilon_0 r \left(\frac{J}{\alpha\sigma_0\varepsilon_0 I_n r} \right)^{n/(n+1)} \tilde{u}_i(\theta, n) \tag{7}$$

where r and θ are the polar coordinates with origin at the crack tip (see Fig. 1), I_n is a dimensionless constant that depends on n, $\tilde{\sigma}_{ij}$, $\tilde{\varepsilon}_{ij}$ and $\tilde{u}_i$ are dimensionless angular functions of θ and n. Let us consider a crack in direction x_1; J (Rice's integral) is then defined by

$$J = \int_{\Gamma} \left(W n_1 - \sigma_{ik} n_k \frac{\partial u_i}{\partial x_1} \right) \mathrm{d}s \tag{8}$$

with Γ a counter-clockwise path around the crack tip, $\mathbf{n}$ the unit outward normal to Γ, $W = \int_0^{\varepsilon_{ij}} \sigma_{ij}\, \mathrm{d}\varepsilon_{ij}$ the strain energy density where σ_{ij} and ε_{ij} are the stress and strain tensors, respectively, and u_i the ith component of the displacement field. The J-integral can be shown to be independent of the Γ contour for finite plasticity, this can be extended to incremental theory if the structure is submitted to an increasing radial loading (see Ref. [17]). One of the objectives of this work is to extend this approach to fatigue crack growth analysis in the case of confined plasticity: if the Γ contour is large enough to totally surround the plastic zone, the independence property should still exist (see Ref. [17]).

Eqs. (5)–(7) represent the HRR fields under pure mode I [9,10] and pure mode II [15,16]. The *tilde* angular functions $\tilde{\sigma}_{ij}(\theta, n)$, $\tilde{\varepsilon}_{ij}(\theta, n)$ and $\tilde{u}_i(\theta, n)$ depend on the material constant n and are different for pure mode I and pure mode II. In Refs. [9,10] these functions are calculated for pure mode I, they can also be calculated for pure mode II considering the anti-symmetry conditions (see Ref. [15]).

2.2. Fourier analysis

As the HRR fields are explicitly known, we choose to introduce them as a new enrichment basis in X-FEM. But, as we have to solve a fourth-order non-linear differential equation to evaluate them (see Refs. [9,10]), we shall approximate them by simpler functions. For the linear elastic case, the asymptotic displacement solutions are

$$u_1(r,\theta) = \frac{1}{2\mu}\sqrt{\frac{r}{2\pi}}\left(K_{\mathrm{I}}\cos\frac{\theta}{2}(k-\cos\theta) + K_{\mathrm{II}}\sin\frac{\theta}{2}(k+\cos\theta+2)\right) \tag{9}$$

$$u_2(r,\theta) = \frac{1}{2\mu}\sqrt{\frac{r}{2\pi}}\left(K_{\mathrm{I}}\sin\frac{\theta}{2}(k-\cos\theta) - K_{\mathrm{II}}\cos\frac{\theta}{2}(k+\cos\theta-2)\right) \tag{10}$$

where k is the Kolosov constant $k = (3-\nu)/(1+\nu)$ for plane stress and $k = 3-4\nu$ for plane strain. These functions can be expanded on the following basis:

$$\left\{\sqrt{r}\sin\frac{\theta}{2}, \sqrt{r}\cos\frac{\theta}{2}, \sqrt{r}\sin\frac{\theta}{2}\sin\theta, \sqrt{r}\cos\frac{\theta}{2}\sin\theta\right\} \tag{11}$$

In the case of elastic–plastic fields, we perform a Fourier decomposition of the functions $\tilde{u}_i(\theta,n)$ for both mode I and mode II. The results given by the solution of Eq. (7) have to be handled. These functions, which are known on the interval $[-\pi;\pi]$, are periodized on $[0;4\pi]$ by conserving the symmetry and anti-symmetry properties of the linear elastic fields, and the variable is taken to be $\theta/2$ instead of θ. After these manipulations, the Fourier analysis of these fields is done using the well-known formulas (for a given scalar function f of a real parameter t):

$$f(t) = a_0 + \sum_{n=1}^{\infty}\left(a_n\cos(n\omega t) + b_n\sin(n\omega t)\right) \tag{12}$$

with

$$a_0 = \frac{1}{T}\int_{\alpha}^{\alpha+T} f(t)\,\mathrm{d}t \tag{13}$$

$$a_n = \frac{2}{T}\int_{\alpha}^{\alpha+T} f(t)\cos(n\omega t)\,\mathrm{d}t \tag{14}$$

$$b_n = \frac{2}{T}\int_{\alpha}^{\alpha+T} f(t)\sin(n\omega t)\,\mathrm{d}t \tag{15}$$

T the period of the function f, α a given real, and n a strictly positive integer.

It appears that the only non-zero harmonics are $\cos(k\frac{\theta}{2})$ and $\sin(k\frac{\theta}{2})$ (for k in $\mathbb{N}$) depending on the symmetry and anti-symmetry properties of the function considered.

The Fourier decomposition of solutions with n values between 1 and 100 shows that the HRR fields can be well approximated by using a truncated Fourier expansion by taking only the first four non-zero harmonics for each function. The Fourier expansion are compared to the complete HRR solution in Fig. 2 for pure mode I and pure mode II under plane strain conditions for three types of material (high hardening $n = 3.7$, medium hardening $n = 10$ and low hardening $n = 50$).

Therefore, we can represent the displacement fields under pure mode I and pure mode II by expanding the HRR functions on the basis given in Eq. (16):

$$r^{1/(n+1)}\left\{\left(\cos\frac{k\theta}{2}, \sin\frac{k\theta}{2}\right);\ k\in[1,3,5,7]\right\} \tag{16}$$

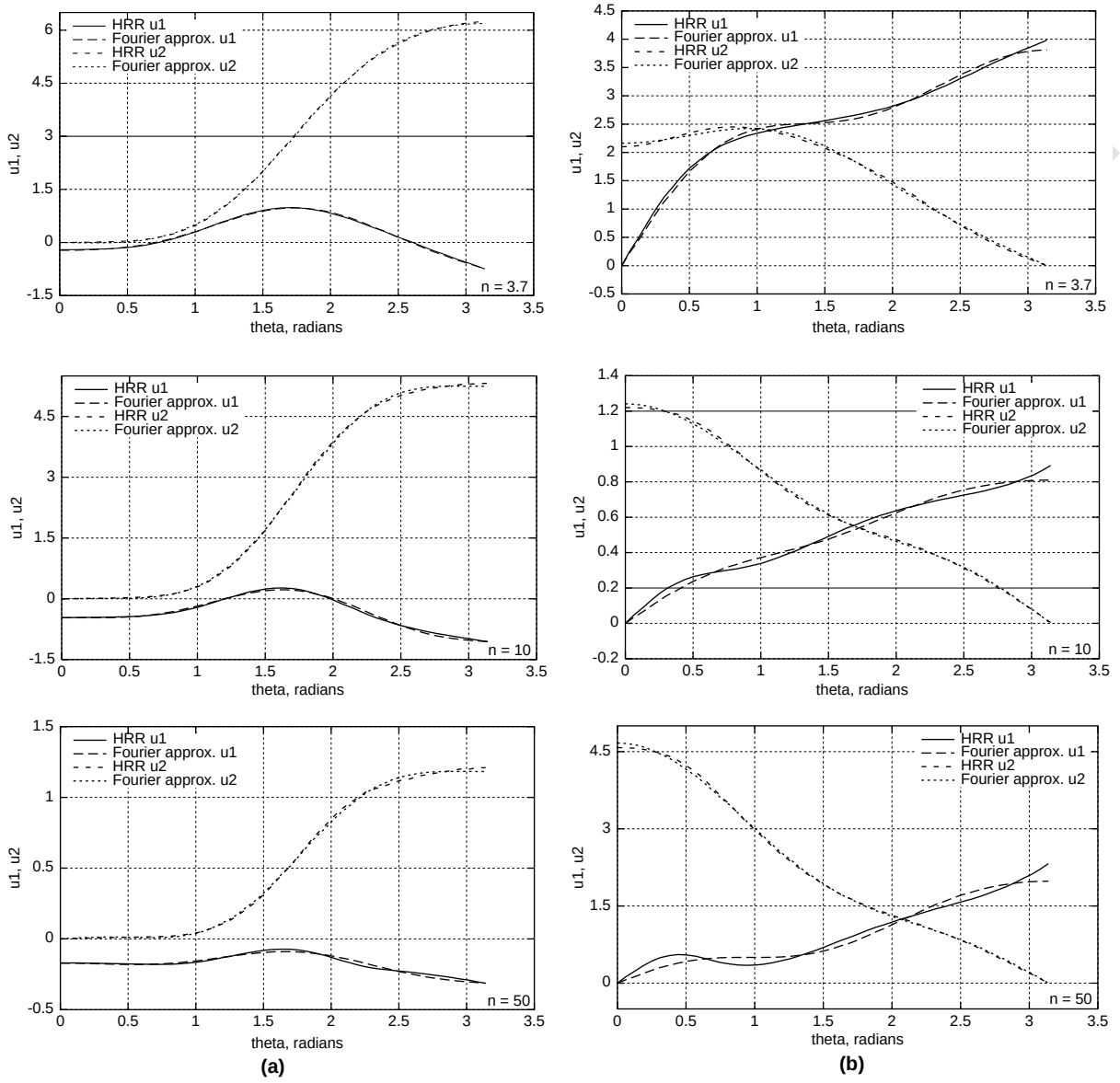

Fig. 2. Approximations of the HRR fields for mode I (a) and mode II (b).

3. Extended finite element enrichment basis

3.1. The extended finite element method—linear elastic case

In the presented method, we use the extended finite element method, first introduced in Refs. [2,3], in which an enrichment basis is added to the classical finite element basis approximation. This is done using the partition of unity method [1]. The enriched basis shape functions are associated to new degrees of freedom and the displacement field can be written (see Ref. [3]):

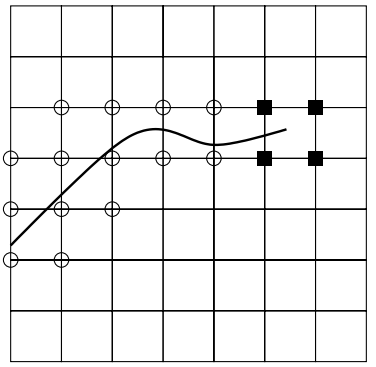

Fig. 3. An arbitrary crack placed on a mesh-enrichment strategy.

$$U = \sum_{i \in \mathcal{N}} N_i(x) U_i + \sum_{i \in \mathcal{N}_{\text{cut}}} N_i(x) H(x) a_i + \sum_{i \in \mathcal{N}_{\text{front}}} \sum_{\alpha} N_i(x) B_\alpha(x) b_{i,\alpha} \tag{17}$$

$\mathcal{N}$ is the set of the standard finite element nodes, $\mathcal{N}_{\text{cut}}$ the set of nodes which belong to elements completely cut by the crack (circled nodes in Fig. 3) and $\mathcal{N}_{\text{front}}$ the set of nodes containing a crack front (square nodes in Fig. 3). N_i are the standard finite element shape functions, H is a function which value is 1 if x is above the crack surface and -1 if x is under the crack surface. $[B_\alpha]$ is derived from the LEFM asymptotic displacement field given in Eqs. (9) and (10), see Ref. [13]:

$$[B_\alpha] = \left[\sqrt{r} \sin\frac{\theta}{2}, \sqrt{r} \cos\frac{\theta}{2}, \sqrt{r} \sin\frac{\theta}{2} \sin\theta, \sqrt{r} \cos\frac{\theta}{2} \sin\theta \right] \tag{18}$$

3.2. Plastic case

The Fourier analysis led to the choice of the enrichment basis given by Eq. (16). The comparison of this basis with the linear elastic one (given by Eq. (18)) induced one to use trigonometric identities in order to have only one function ($\sin\theta/2$) with discontinuity between $\theta = +\pi$ and $\theta = -\pi$. As ill conditioning of the stiffness matrix appears, one has to improve the numerical integration and to limit the dimension of the enrichment basis.

3.2.1. Numerical integration

The numerical integration of the weak form proposed for linear solutions must be improved because of the existence of high order trigonometric Fourier terms in the basis functions in case of plasticity. The subtriangle partitioning already used in X-FEM (see Ref. [3]) which consists in partitioning the elements cut by the crack into subtriangles (each with 3 Gauss quadrature points) is not sufficient.

One could have increased the number of quadrature points in each subtriangle to improve the numerical integration of the high order terms, but one has to keep in mind the problem of propagation. If the crack propagates in a new direction, the subtriangles associated with the previous crack position will also be partitioned into new subtriangles to be coherent with the new crack faces (see Fig. 4). With this technique, the projection of the stress and internal variable fields is inevitable as the crack propagates, which can lead to problems such as the non-conservation of the energy. Therefore, a new efficient integration scheme that could circumvent this problem must avoid a new partitioning of an element as the crack propagates.

One chooses to use a simple subquadrangle partitioning technique equivalent to the one proposed in Ref. [8]. The elements cut by the crack are subdivided into 16 subquadrangles with 16 Gauss quadrature points

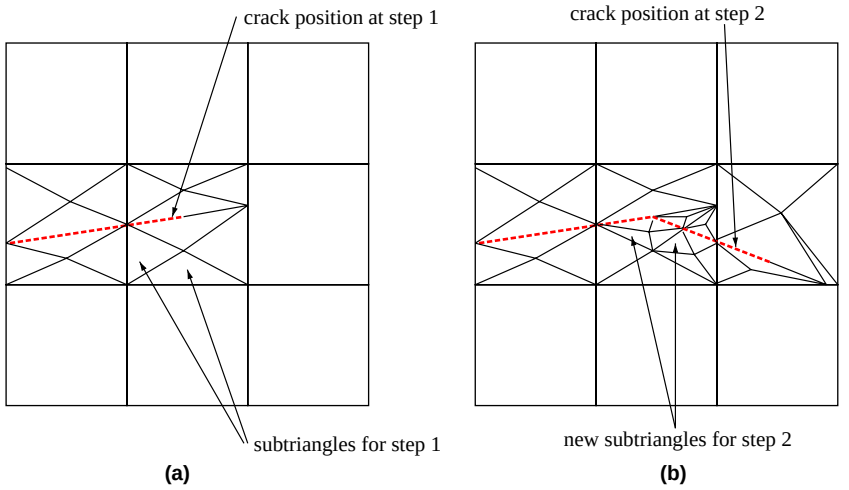

Fig. 4. Subtriangles (a) before propagation and (b) after propagation.

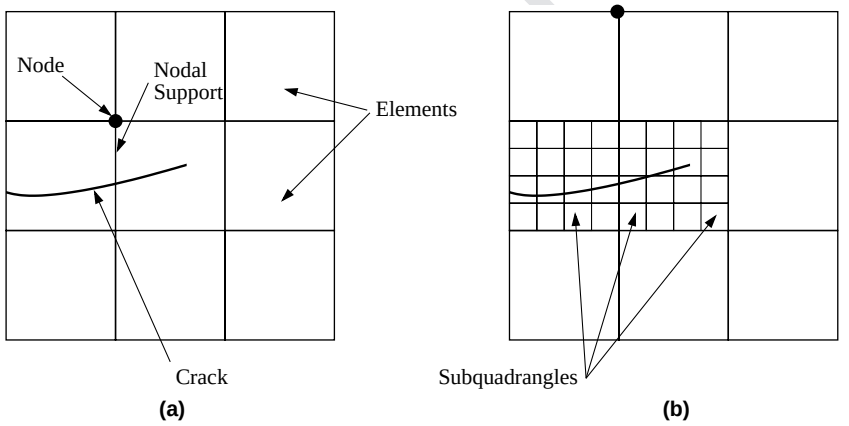

Fig. 5. (a) Nodal support cut by a crack, (b) the subquadrangles associated with elements cut by the crack.

in each subquadrangle (see Fig. 5). With this technique the subelements edges are not compatible with the crack faces, and integration errors may appear because of the enrichment functions that are discontinuous on the crack faces (i.e., the jump function H and the tip function $\sin(\theta/2)$).

Therefore, one chooses to create two sets of subelements based on the subquadrangles grid (see Fig. 6): one set (denoted by (a) and (b) in Fig. 6), which is compatible with the crack faces,[1] to calculate the stiffness matrix for (a) the elements totally cut by the crack (i.e., enriched with the jump function H) and (b) the element containing the crack front; and another set (denoted by (c) and (d) in Fig. 6), which is independent of the crack faces, to compute the plastic flow in each element cut by the crack ((c) for the elements totally cut by the crack and (d) for the element containing the crack front).

[1] The subquadrangles cut by the crack are replaced by subtriangles obtain with the same technique as in the elastic case.

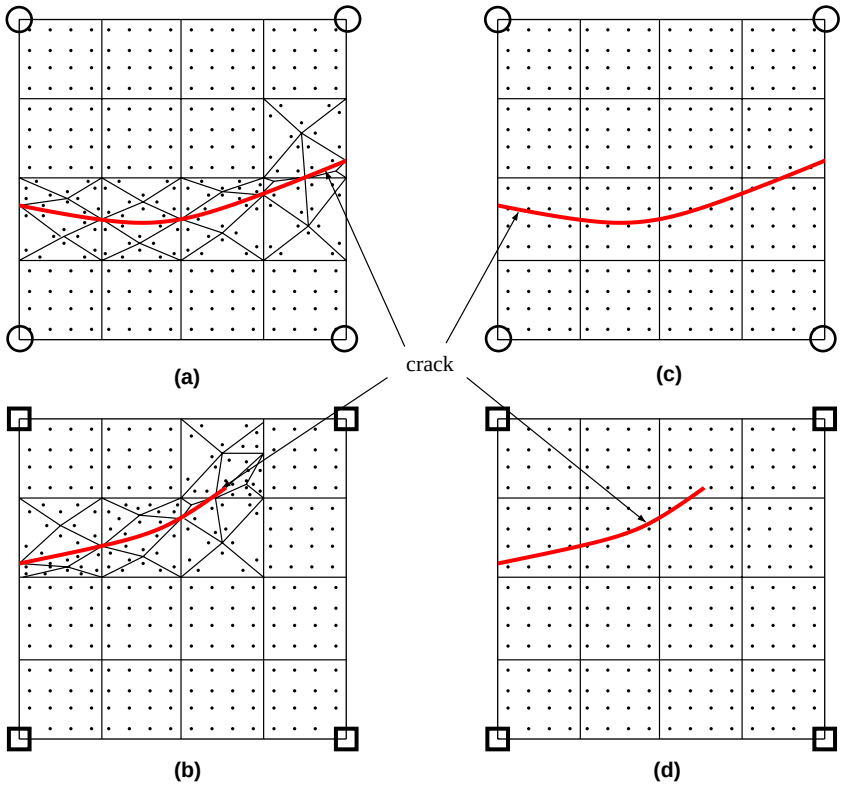

Fig. 6. Partitioning for the evaluation of (a) discontinuous stiffness matrix, (b) tip stiffness matrix. Partitioning for plastic flow computation for (c) discontinuous element and (d) tip element.

3.2.2. Study of the basis

Three bases, given in Eqs. (19)–(21), are tested. A comparison of the numerical rank of the tip stiffness matrix is made for these three bases for the element containing the crack front (see Fig. 7):

$$\text{(a)}\quad r^{1/(n+1)}\left\{\sin\frac{\theta}{2},\cos\frac{\theta}{2},\sin\frac{\theta}{2}\sin\theta,\cos\frac{\theta}{2}\sin\theta,\sin\frac{\theta}{2}\sin 2\theta,\cos\frac{\theta}{2}\sin 2\theta\right\} \tag{19}$$

$$\text{(b)}\quad r^{1/(n+1)}\left\{\sin\frac{\theta}{2},\cos\frac{\theta}{2},\sin\frac{\theta}{2}\sin\theta,\cos\frac{\theta}{2}\sin\theta,\sin\frac{\theta}{2}\sin 3\theta,\cos\frac{\theta}{2}\sin 3\theta\right\} \tag{20}$$

$$\text{(c)}\quad r^{1/(n+1)}\left\{\sin\frac{\theta}{2},\cos\frac{\theta}{2},\sin\frac{\theta}{2}\sin\theta,\cos\frac{\theta}{2}\sin\theta,\sin\frac{\theta}{2}\sin 2\theta,\cos\frac{\theta}{2}\sin 2\theta,\sin\frac{\theta}{2}\sin 3\theta,\cos\frac{\theta}{2}\sin 3\theta\right\} \tag{21}$$

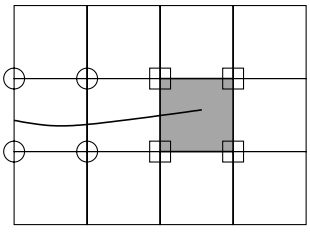

Fig. 7. Finite element containing the crack front.

Table 1
Numerical rank of the stiffness matrix for different enrichment strategies

Enrichment basis	Numerical rank of K_{el}
Elastic (Eq. (18))	4
(a)	8
(b)	4
(c)	12

What is called the numerical rank is defined as follows: let $\mathscr{A}$ be the set of the eigenvalues of a stiffness matrix $\mathbb{K}$, $\mathscr{A}$ can be subdivided into three sets listed in Eq. (22) (with $E \sim 10^{11}$ Pa and $v \sim 0.3$).

$$\mathscr{A} = \begin{cases} \mathscr{A}_{\text{nul}} = [a \in \mathscr{A};\ |a| \backsim 10^{-14}] \\ \mathscr{A}_{\text{hourglass}} = [a \in \mathscr{A};\ |a| \backsim 10^{-4}] \\ \mathscr{A}_{\text{norm}} = [a \in \mathscr{A};\ |a| \backsim 10^{8}] \end{cases} \tag{22}$$

The eigenvectors associated to the eigenvalues in $\mathscr{A}_{\text{nul}}$ (respectively $\mathscr{A}_{\text{norm}}$) correspond to the rigid body motion (respectively to the transmissible modes). The ones associated to the eigenvalues in $\mathscr{A}_{\text{hourglass}}$ are associated to "hourglass" like modes, and the numerical rank is defined as the dimension of $\mathscr{A}_{\text{hourglass}}$.

The results given in Table 1 indicate that with bases (a) and (c) the stiffness matrix has 8 or 12 "hourglass" modes. The "hourglass" behavior is also present for the basis (b) but there are only four modes which seem not to be transmissible (see Ref. [18] where the case of discontinuous enrichment is studied), as for the elastic basis. The ill-conditioning problem and the presence of these "hourglass" modes has already been pointed out in the literature: see Ref. [19] for the conditioning study and Refs. [18,20] for the "hourglass" modes.

Therefore, one chooses to use the basis (b) given by Eq. (20), which appears to be the same as the one proposed in [14] in the context of the element free Galerkin method.

4. Numerical examples

All the numerical examples presented below are treated in plane strain conditions.

4.1. Pure mode I

The first comparison is made for a pure mode I SE(T) specimen between a 380 four nodes quadrangles mesh in X-FEM with 548 degrees of freedom (DOF) and a 892 six nodes triangles mesh in a classical finite element code with 4106 DOFs. The geometry and the meshes are given in Fig. 8, with the values $W = 20$ cm, $L = 25$ cm and $a = 10$ cm. The specimen is monotically put in tension with an increasing load and then monotically brought back to zero load with the same number of steps.

The usual incremental plasticity theory is used to predict stress and strains history. The comparison is made for two materials, one with strong hardening ($n = 3.7$) and one with weak hardening ($n = 30$). One compares the displacement jump (denoted by $[u]$) between the crack faces evaluated at the intersection of the crack faces and the boundary of the element containing the crack front, in the normal direction

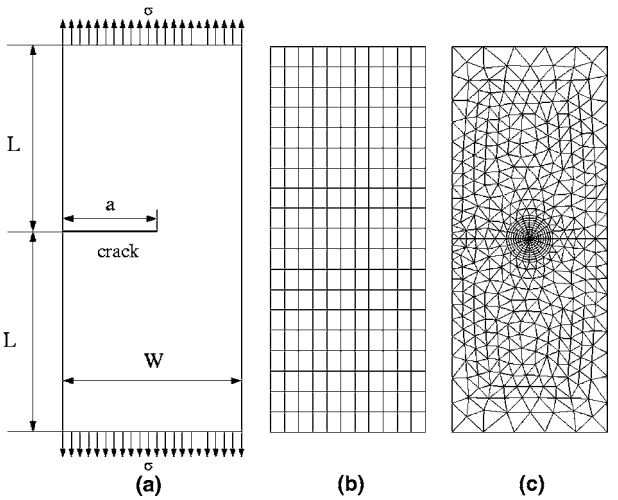

Fig. 8. (a) Geometry of the SE(*T*) specimen, (b) meshes used in X-FEM and (c) classical finite element.

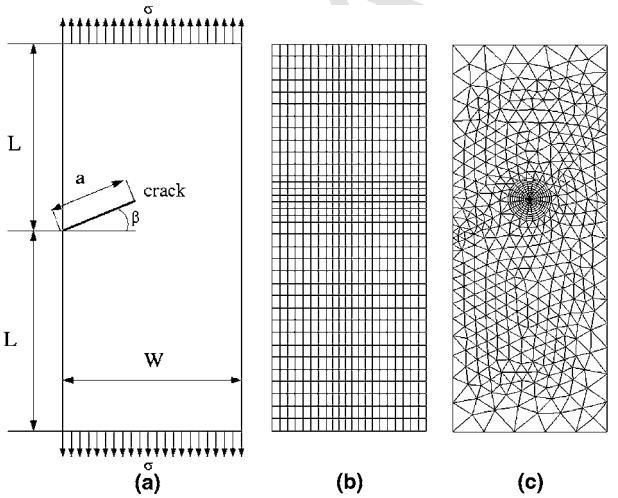

Fig. 9. (a) Geometry of the SE(*T*) specimen, (b) meshes used in X-FEM and (c) classical finite element.

to the crack faces, and the *J*-integral. The results are shown in Fig. 10 for [*u*] and Fig. 11 for *J*. One plots the quantities [*u*] and *J* versus the evolution factor (computational step) and the normalized variation between the FE and X-FEM results in percent versus the evolution factor on the same figure.

The results are very close for both [*u*] and *J* even when the load is decreasing. The displacement jump [*u*] is slightly bigger with X-FEM than with a usual finite element analysis. One can see the residual opening of the crack due to plastic strains when the load comes back to a zero value in Fig. 10.

The same comparison is made without the new plastic tip enrichment in X-FEM i.e., only with discontinuous enrichment. The *J*-integral results can be found in Fig. 12. These results (about 50% of variation at

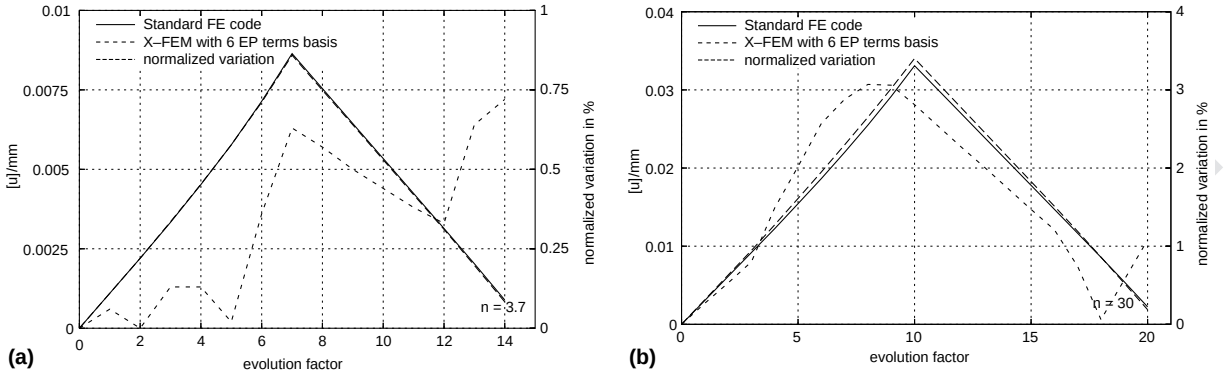

Fig. 10. Comparison for the displacement jump [u] for $n = 3.7$ (a) and $n = 30$ (b) in plane strain pure mode I.

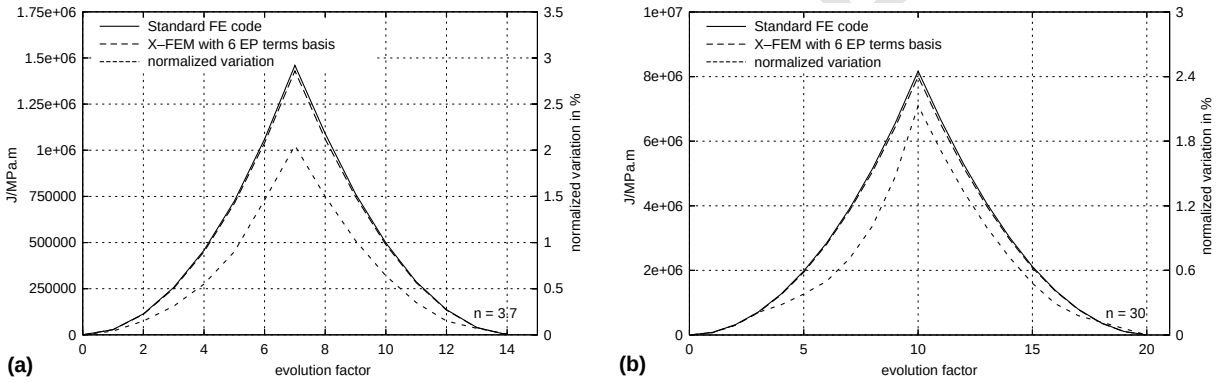

Fig. 11. Comparison for the J-integral for $n = 3.7$ (a) and $n = 30$ (b) in plane strain pure mode I.

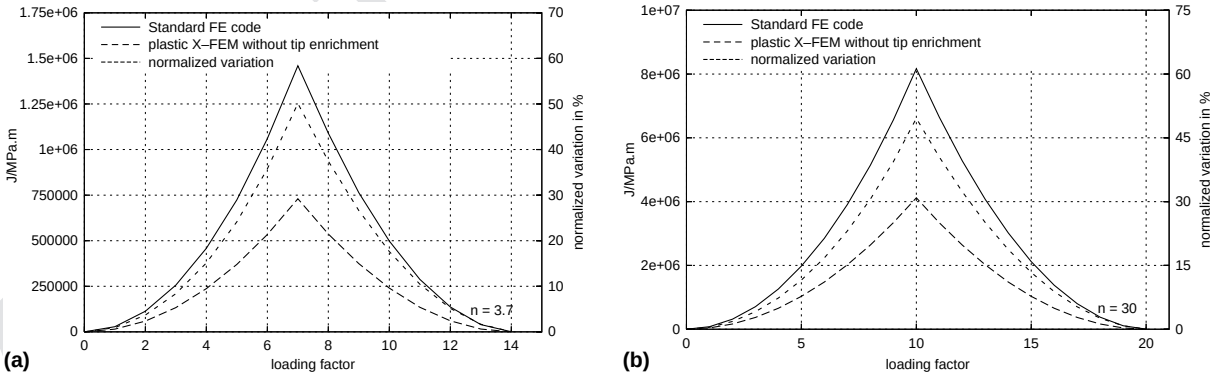

Fig. 12. Comparison for the J-integral without plastic tip enrichment for $n = 3.7$ (a) and $n = 30$ (b) in plane strain pure mode I.

the maximum load) show that the new plastic tip enrichment is absolutely necessary to treat the material non-linearities at the vicinity of a crack.

4.2. Mixed mode

4.2.1. Comparison with a usual elastic–plastic finite element calculation

The second comparison is made for a mixed mode SE(T) specimen with an inclined crack. The geometry and the meshes are given in Fig. 9, with the following parameters $W = 20$ cm, $L = 25$ cm and $a = 11.18$ cm, $\beta = 26.5°$. The comparison is also made for two materials, with high hardening ($n = 3.7$) and low hardening ($n = 30$), for the displacement jump $[u]$ and the J-integral. The specimen is monotically submitted to an increasing load. One plots the quantities $[u]$ and J versus the loading factor (computational step) and the variation between the FE and X-FEM results in percent versus the loading factor on the same figure. The results are shown in Figs. 13 and 14. The two computations compare quite well (less than 2.5% of variation in all cases).

4.2.2. Comparison with elastic X-FEM calculation

The comparison is also made, for the same specimen, on the stress intensity factors (SIF). One compares the SIFs calculated with an elastic behavior and an elastic enrichment basis to the ones calculated with an elastic–plastic behavior and the plastic enrichment basis introduced earlier. In both case the SIFs are calculated with the interaction integral method presented in Refs. [2,3]. In this method, the linear elastic asymptotic fields are used as auxilliary fields to uncouple the SIFs.

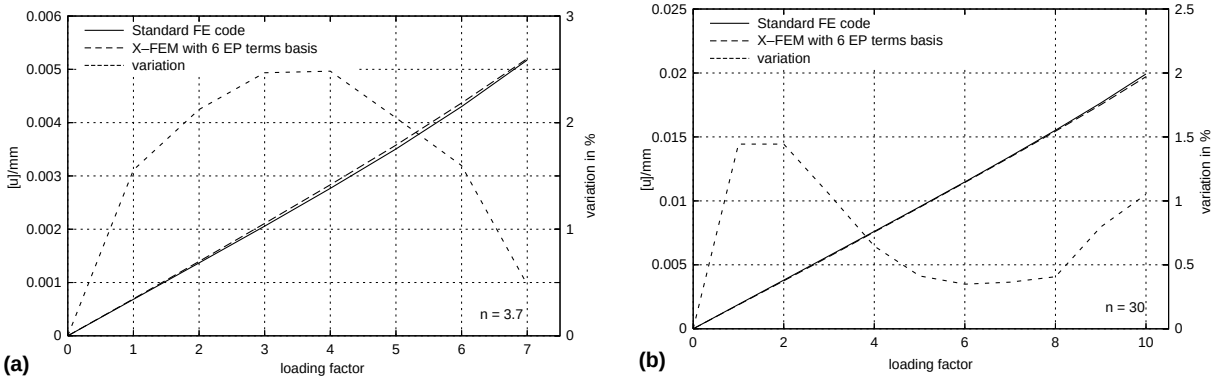

Fig. 13. Comparison for the displacement jump $[u]$ for $n = 3.7$ (a) and $n = 30$ (b) in plane strain mixed mode.

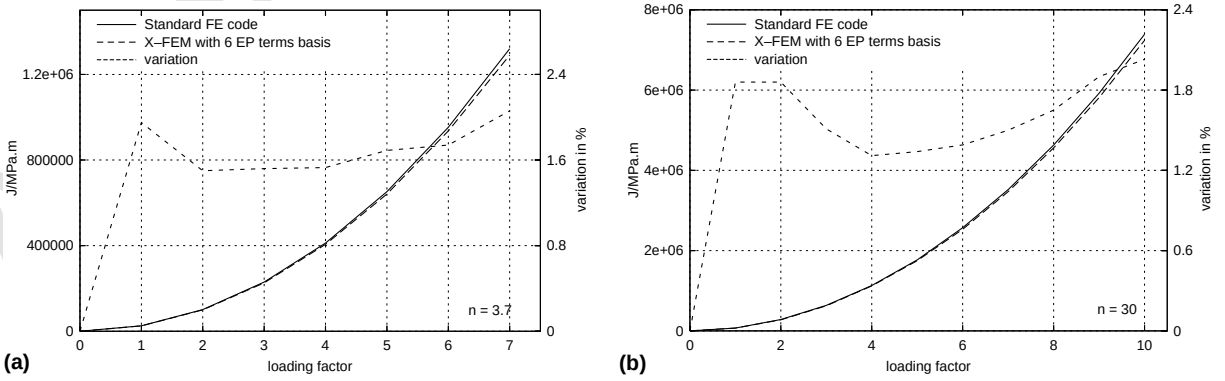

Fig. 14. Comparison for the J-integral for $n = 3.7$ (a) and $n = 30$ (b) in plane strain mixed mode.

A weighting function $q(\mathbf{x})$ is used for the calculation of the interaction integral which takes a value of unity on an open set containing the crack tip and vanishes on an outer prescribed contour C_0 (see Fig. 16). As it is the gradient of q that counts in the interaction integral, the only elements that produce a non-zero value are the ones located at the boundary of C_0. With the hypothesis of confined plasticity, plastic strains are only present on the element containing the crack front, i.e., in an element that produces a zero value in the interaction integral. Therefore, one can use the same method for evaluating the SIFs in the elastic–plastic case.

The results are shown in Fig. 15 for two materials (n = 3.7 and 30). One can observe in Fig. 15 a loss of linearity for the plastic cases after step number 2 which is the one where plasticity appears. As the difference between elastic and plastic SIFs is not considerable one sees that the hypothesis of confined plasticity is relevant. Furthermore, these results show that even in the case of confined plasticity (i.e., not so far from the LEFM conditions), when the load is such that plasticity appears, the non-linearity is also present on the SIFs and that the elastic prediction under estimates them.

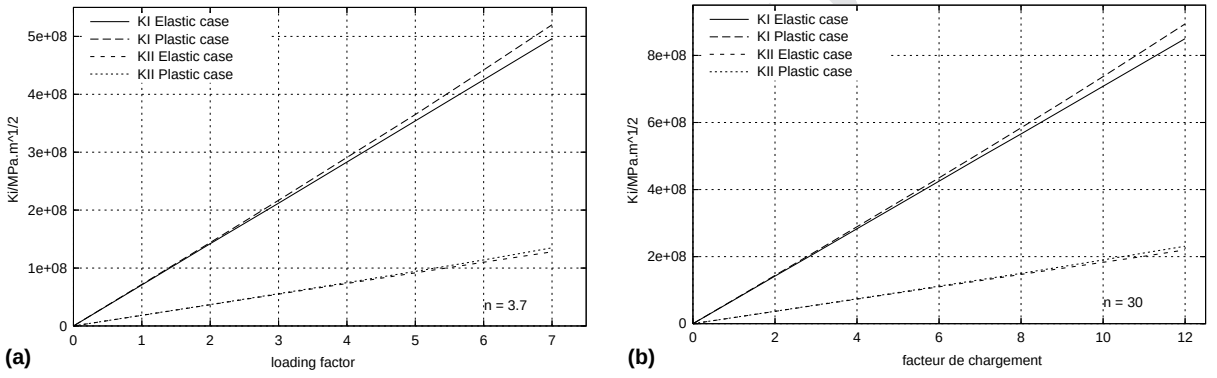

Fig. 15. Comparison of the SIFs between elastic and elasto-plastic case for n = 3.7 (a) and n = 30 (b) in plane strain.

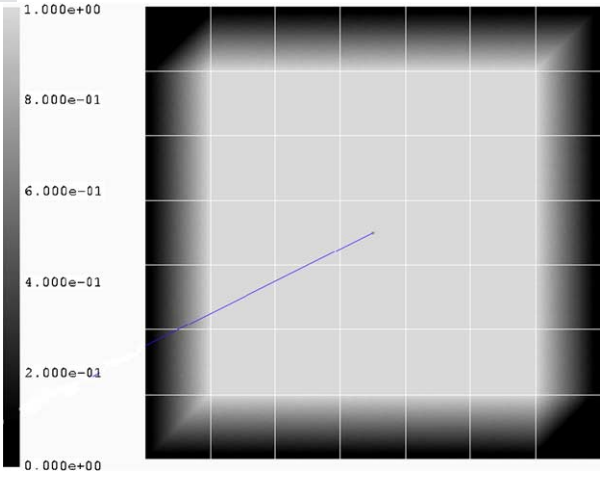

Fig. 16. Weight function q on the elements with an inclined crack.

5. Conclusion

A method has been presented for enriching finite elements approximations in the framework of EPFM. The main hypothesis of this study is that we only consider the case of confined plasticity i.e., one only enriches the element containing the crack front. A new plastic enrichment basis, that captures well the HRR plastic singularities, is presented in the framework of the X-FEM, coupled with a Newton like iterative algorithm and a radial return mapping scheme to compute plastic flow. As discussed before, this study is done in the context of confined plasticity and will be used to predict elastic–plastic fatigue crack growth without remeshing.

The results presented show very good accuracy for numerical evaluation of standard fracture parameters such as *J*-integral. In the first example the presented method shows a good accuracy when the load is increasing (which shows that the plastic solution is well captured by the new tip enrichment basis) as well as when unloading appears. This last result shows the ability of the presented method for fatigue crack analysis. In the last example, the influence of material non-linearities in the evaluation of stress intensity factors is demonstrated in the case of confined plasticity i.e., not so far from the LEFM conditions.

This improvement in X-FEM fracture calculation will be applied to predict mixed mode fatigue crack growth. The new partitioning integration strategy will therefore be adapted to avoid the projection of internal variables as the crack propagates. The main idea of this modification will be to partition with the same technique a bigger set of elements that surround the crack tip, in order to initialize internal variables while in elastic conditions.

Acknowledgment

The authors are grateful for the support of the Délégation Générale pour l'Armement and the Centre Technique des Industries Mécaniques.

References

[1] I. Babuška, J.M. Melenk, The partition of unity method, Int. J. Numer. Methods Engrg. 40 (1997) 727–758.
[2] T. Black, T. Belytschko, Elastic crack growth in finite elements with minimal remeshing, Int. J. Numer. Methods Engrg. 45 (1999) 601–620.
[3] N. Moës, J. Dolbow, T. Belytschko, A finite element method for crack growth without remeshing, Int. J. Numer. Methods Engrg. 46 (1) (1999) 133–150.
[4] N. Sukumar, N. Moës, B. Moran, T. Belytschko, Extended finite element method for three-dimensional crack modelling, Int. J. Numer. Methods Engrg. 48 (1999) 1549–1570.
[5] R. Huang, J.H. Prévost, Z.Y. Huang, Z. Suo, Channel-cracking of thin films with the extended finite element method, Engrg. Fracture Mech. 70 (2003) 2513–2526.
[6] P.M. Mariano, F.L. Stazi, Strain localization due to crack-microcrack interactions: X-FEM for a multified approach, Comput. Methods Appl. Mech Engrg. 193 (2004) 5035–5062.
[7] G.N. Wells, R. de Borst, L.J. Sluys, A consistent geometrically non-linear approach for delamination, Int. J. Numer. Methods Engrg. 54 (2002) 1333–1355.
[8] H. Ji, D. Chopp, J.E. Dolbow, A hybrid finite element/level set method for modelling phase transformation, Int. J. Numer. Methods Engrg. 54 (2002) 1209–1233.
[9] J.W. Hutchinson, Singular behavior at the end of a tensile crack in a hardening material, J. Mech. Phys. Solids 16 (1968) 13–31.
[10] J.R. Rice, G.F. Rosengren, Plane strain deformation near a crack tip in a power-law hardening material, J. Mech. Phys. Solids 16 (1968) 1–12.
[11] N.P. O'Dowd, C.F. Shih, Family of crack-tip fields characterized by a triaxiality parameter: Part I—structure of fields, J. Mech. Phys. Solids 39 (8) (1991) 989–1015.
[12] N.P. O'Dowd, C.F. Shih, Family of crack-tip fields characterized by a triaxiality parameter: Part II—fracture applications, J. Mech. Phys. Solids 40 (5) (1992) 939–963.

[13] M. Fleming, Y.U. Chu, B. Moran, T. Belytschko, Enriched element-free Galerkin methods for crack tip fields, Int. J. Numer. Methods Engrg. 40 (1997) 1483–1504.
[14] B.N. Rao, S. Rahman, An enriched meshless method for non-linear fracture mechanics, Int. J. Numer. Methods Engrg. 50 (2004) 197–223.
[15] J. Pan, Asymptotic analysis of a crack in a power-law material under combined in-plane and out-of-plane shear loading conditions, J. Mech. Phys. Solids 38 (2) (1990) 133–159.
[16] J. Pan, C.F. Shih, Elastic–plastic analysis of combined mode I, II and III crack-tip fields under small-scale yielding conditions, Int. J. Solids Struct. 29 (22) (1992) 2795–2814.
[17] G. Pluvinage, Mécanique élasto-plastique de la rupture—Critères d'amorçage, Cepadues Editions, 1989.
[18] S. Mariani, U. Perego, Extended finite element method for quasi-brittle fracture, Int. J. Numer. Methods Engrg. 58 (2003) 103–126.
[19] C.A. Duarte, I. Babuška, J.T. Oden, Generalized finite element methods for three-dimensional structural mechanics problems, Comput. Struct. 77 (2000) 215–232.
[20] P. Laborde, J. Pommier, Y. Renard, M. Salaün, High order extended finite element method for cracked domains, Int. J. Numer. Methods Engrg., submitted.